Draft version June 13, 2023
Typeset using LaTeX default style in AASTeX631

PHYS134L: Discovery of WASP-14b via Transit Photometry

[1] *Department of Physics, University of California, Santa Barbara, CA 93106*

(Dated: June 13, 2023)

ABSTRACT

Exoplanet research consists of detecting foreign planets beyond our solar system that may very well host habitable life or can host habitable life. To do so, astronomers employ a plethora of detection methods. In this paper, we will employ one of many detection methods, transit photometry, to detect the presence of WASP-14b, a gas-giant exoplanet that orbits an F-type star with apparent magnitude 9.745 ± 0.004 Joshi et al. (2009a) Institute (2023a). And after collecting and reducing the banzai images of WASP-14, we were able to produce a favorable calibrated light curve that indicates a loss of 0.10 in magnitude. A result that compares well to existing literature circulating WASP-14b.

Keywords: Theme: Exoplanets — Transit Photometry, Planet Occulation — Target: WASP-14b, GJ-1214b – Star: WASP-14, GJ-1214

1. INTRODUCTION

The field of exoplanet research is a relatively new field of physics blooming with new discoveries near the second via a wide variety of discovery methods. However, the discovery of planets beyond our solar system via planet occultation or as it is sometimes better known as, transit photometry, is the discovery of a possible faint companion orbiting its host star by observing the amount of light loss over time using a light curve (see fig. 1) Society (2023).

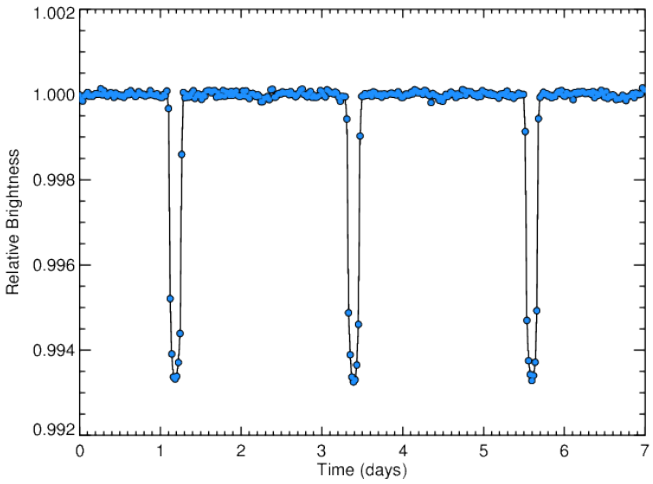

Figure 1. A Kepler light curve of exoplanet HAT-P-7 b. A hot Jupiter which makes it one of the easiest types of exoplanets to detect - perfect exoplanet candidate to exemplify a transit light curve. A plot of time (in days) on the x-axis versus relative brightness on the y-axis. As seen, the entire span of the graph is within 1% - i.e. extremely precise brightness measurements Vanderburg (2020)

.

Figure 1, for example, is a perfect illustration of the capabilities of a light curve that tracks these dips or loss of magnitudes over time when the planet passes in front of its host star. This in practice allows astronomers to determine the presence of possible faint companions, the possible size of the faint companion, the orbital period (if successive transits are visible), and transit duration NASA (2017). Most importantly, detection methods such as transit photometry and others allow astronomers to further corroborate on planetary formation and evolution models and answer one of humanity's longest-standing questions - are we alone in the universe?

In this paper, we will produce and analyze the transit light curves of both GJ-1214b and WASP-14b. The selection of these two exoplanet candidates was based on our initial judgment formed with the help of the Las Cumbres Observatory (LCO) Visibility Tool and the NASA Exoplanet Watch Target List (LCO) NASA (2023). We will then compare our resulting light curves to those from existing literature to note how well we were able to produce a light curve for both exoplanet candidates.

2. EXOPLANET TARGETS

2.1. *GJ-1214b*

GJ-1214b is a super-Earth exoplanet orbiting an M-type star, GJ-1214, with an apparent magnitude of 15.1 ± 0.2 (see fig. 2) Charbonneau et al. (2009) Institute (2023b). Discovered in December 2009, GJ-1214b was part of a project known as MEarth, which used robotic telescopes to observe M-dwarf stars for the potential existence of Earth-like exoplanets through Transit Photometry. It is observed to have a mass 6.55M$_{Earth}$, a radius 2.68R_{Earth} with a 1.58-day orbit Charbonneau et al. (2009). Ice giants typically have a range of radius 2R_{Earth} to 6R_{Earth}, making GJ-1214b an intermediary between Earth and an ice giant Charbonneau et al. (2009).

Figure 2. Raw image of the GJ-1214 star centered on the image displayed using DS9 - an image display and visualization tool for astronomical data. The limited contrast between the GJ-1214 and its background is a major concern addressed in the forthcoming "Results" and "Discussion" Section.

Moreover, GJ-1214b is of particular interest because sub-Neptunes such as GJ-1214b may have a diversity of compositions from rocky to gas-rich as expected from planetary formation and evolution models. And thus, the history of how a planet accreted or outgassed its atmosphere can be best studied if further constraints on sub-Neptune planets (e.g. GJ-1214b) were made Hood et al. (2020).

2.2. *WASP-14b*

WASP-14b is a gas-giant exoplanet orbiting an F-type star, WASP-14, with an apparent magnitude of 9.745 ± 0.004 (see fig. 3) Joshi et al. (2009a) Institute (2023a). Discovered in 2008 using Transit Photometry, it is observed to have a mass of 7.3$M_{Jupiter}$ and a 2.24-day orbit. Transiting hot Jupiter such as WASP-14b entails high levels of incident flux, slow rotation, and potentially large temperature gradients Wong et al. (2015).

Moreover, WASP-14 is of particular interest because it is one of the most massive transiting planets that still has no firm explanation about the formation of such highly massive planets with unusually large eccentric orbit for their short orbital period. This, thus, poses a great challenge for theoretical planetary formation and evolution models to explain their internal structure, atmospheric dynamics, and heat distribution Joshi et al. (2009a)

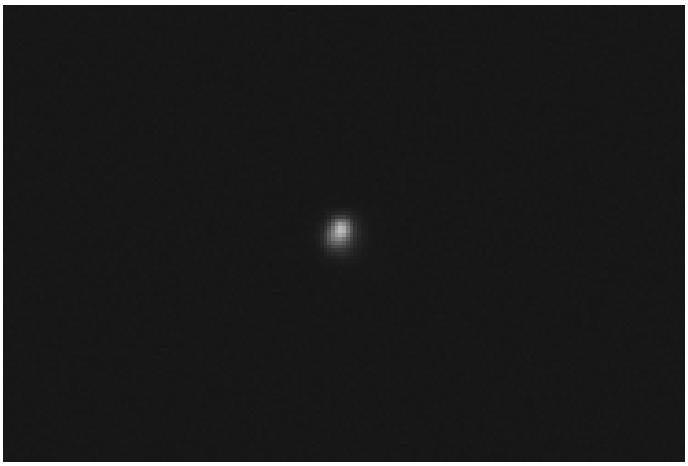

Figure 3. Raw image of the WASP-14 star centered on the image displayed using DS9 - an image display and visualization tool for astronomical data. The stark contrast between WASP-14 and its background is a major indication of success that will be further detailed in the forthcoming "Results" and "Discussion" section.

3. METHODS

3.1. *Transit Photometry Method*

Transit Photometry method heavily depends on taking the light flux of the target star and comparing these values to other stars in the same patch of sky. This is primarily done using digital CCD (Charged Couple Devices) earth-based cameras to gather the information. The camera is then set up and aimed at the target stars region of the sky and pictures before, after, and during the predicted transit. These images are then used to generate a data set of flux values for every frame taken during the session Afanasev (2018).

3.2. *Aperture Photometry*

Aperture Photometry is the process of calibrating the aperture of the target and the surrounding comparison stars. This is done to adjust any uncertainties located in the aperture region. This is typically done by setting an annulus/ring around the perimeter of the target star and one larger surrounding the area of the target star - including about 30-40 pixels out Afanasev (2018)

3.3. *Signal-to-Noise Ratio*

Both GJ-1214 and WASP-14 were first deemed as viable imaging targets by computing the "Signal to Noise Ratio", sometimes denoted as "SNR". The SNR is the ratio of incident flux that is due to the object being observed and the random flux from other sources that acts to corrupt the image Lubin (2022). Thus. a high SNR value is most desired when attempting to produce desirable images of your target. Using equation 1, one would be able to then compute an SNR value:

$$\frac{S}{N} = \frac{FA_\epsilon \tau}{[N_R^2 + \tau N_T]^{1/2}} \tag{1}$$

where F is the point source signal flux on telescope (photon s^{-1} cm^{-2}), A is the telescope area (cm^2, τ is the integration time (s), N_R is the readout noise (e^-), and N_T is the time-dependent noise per unit time Lubin (2022).

We, on the other hand, proceeded to calculate the SNR for both systems by first calculating the transit depth of each system - the ratio between the planet's radius and the star's radius squared NASA (2017).

$$\delta = \left(\frac{R_{planet}}{R_{star}}\right)^2 \tag{2}$$

Next, is to compute the SNR of the star (i.e. $\left(\frac{S}{N}\right)_{star}$) using the LCO SNR calculator and parameters of the star and of our observation request - magnitude of the star and exposure time (LCO). Do note that the exposure time is calculated by multiplying the integration time and the number of exposures - parameters both listed on the observation

request log. The LCO SNR calculator, thus, printed SNR values of 559.3 and 10471 for both GJ-1214 and WASP-14, respectively.

Now with all the necessary variables, the signal to noise ratio of an exoplanet orbiting a star is defined as:

$$\left(\frac{S}{N}\right)_{planet} = \delta \times \left(\frac{S}{N}\right)_{star} \tag{3}$$

GJ-1214B

To observe GJ-1214b, we used Los Cumbres Cerro Tololo Observatory on May 8, 2023: 12:30 am - 2:30 am UTC. Our data set consists of 360 exposures with an integration time of 10 seconds. The 0.4-meter Telescope was assigned with an SDSS-i' filter to the coordinates: Right Ascension 17:15:18.9 and Declination +04:57:50.06. The filter was set to infrared because GJ-1214 b orbits an M-dwarf star which tend to have dimmer luminosity, with a temperatures between 2,000–3,500 K. As a result, their radiation is largely within the infrared range of the electromagnetic spectrum.

Target Name	RA (J2000)	Dec (J2000)	Filter	# Exposures	Integration Time (s)	Observational Windows
GJ-1214	17:15:18.9	+04:57:50.06	SDSS-ip	360	10	May 8, 2023: 12:30 am - 2:30 am (UTC) (South America)

Table 1. Observation request log that was submitted on Wed. May 3, 2023.

And using the parameters listed above, we first calculated an SNR value for GJ-1214 of 559.3. Do note that an SNR value of about 700 is ideal for the telescopes to be able to resolve the target. Another indication of how poor GJ-1214 will be in order to produce a favorable light curve and, thus, detect the presence of GJ-1214b. Likewise, the transit depth, after collecting the planet and star radius and using eqn. 2, is 1.51%. Thus, this leads to an SNR value for GJ-1214b, after using eqn. 3 is 844.543.

WASP-14B

To observe WASP-14b, we used Los Cumbres Observatory for May 17, 2023: 11:30 – 16:30 UTC- North America. Our data set consists of 360 exposures and an integration time of 10 seconds. A 0.4-meter telescope was assigned with SDSS-g' filter to the coordinates: Right Ascension 14:33:06.0 and Declination +21:53:41. For this class of star, the g-filter is best because the exoplanet orbits an F-type star which tend to be within 6,000–7,400 K and as a result, emit a large amount of radiation within the green visible spectrum.

Target Name	RA (J2000)	Dec (J2000)	Filter	# Exposures	Integration Time (s)	Observational Windows
WASP-14	14:33:06.0	+21:53:41	SDSS-g'	360	10	May 17, 2023: 11:30 am - 16:30 am (UTC) (North America)

Table 2. Observation request log that was submitted on Tue. May 16, 2023.

And using the parameters listed above, we first calculated an SNR value for WASP-14 of 10471. Certainly well over the ideal SNR value of 700 for the telescopes to be able to resolve the target. Likewise, the transit depth, after collecting the planet and star radius and using eqn. 2, is 0.975%. Thus, this leads to an SNR value for WASP-14b, after using eqn. 3 is 1029.225.

3.4. *Photometry*

To perform photometry on the images, the open-source astropy package is used to import and extract data from the uncompressed banzai images in Python. Additionally, the Photutils package is used to detect sources in the images (i.e. photutils.detection) and perform aperture photometry (i.e. photutils.aperture).

First step is to find the number of stars, and their positions (x,y coordinates) in a single banzai image. The banzai imagine is first displayed in a gray-scale color-map, with the image data logarithmically transformed to see the variance of the pixels better. The resultant image is seen in figure 4 and figure 5 (see fig. 4 and fig. 5).

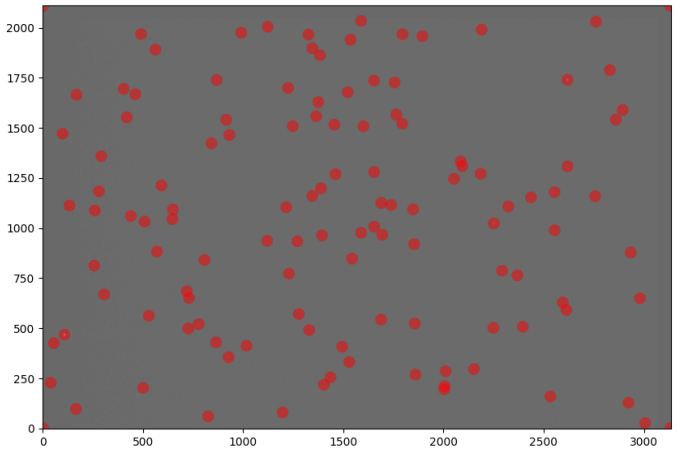

Figure 4. 117 sources were identified using the DAOStarFinder tool from Photoutils for GJ-1214b

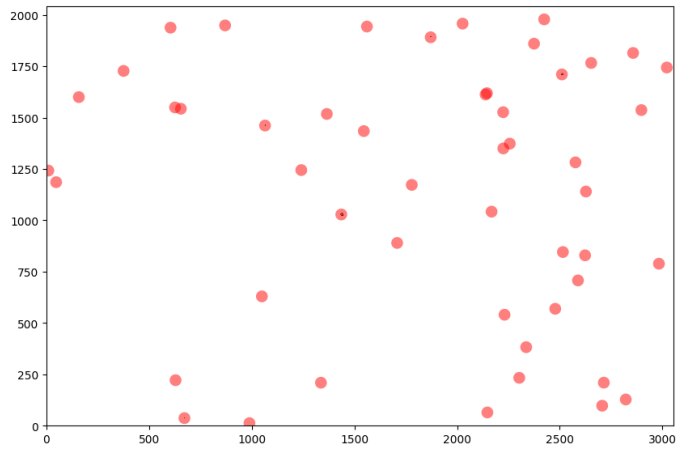

Figure 5. 50 sources were identified using the DAOStarFinder tool from Phototulis for WASP-14

Next, a sigma clip is used to exclude values 3.0 standard deviations away as background estimation to exclude bright sources. The background estimator is set to the MedianBackground() due to its robustness to outliers and image noise. The DAOStarFinder from Phototutils is used to detect smaller and fainter sources within the image. The full width half maximum of the gaussian kernel is set to 5 with a threshold of 5σ. The threshold helps determines what is considered as a source within the image. Using a circular aperture tool with a radius of 15 pixels, the photon count of each source is obtained. The sources are all plotted and a .csv file containing all star positions and aperture sums is created.

Next, extract the data from all banzai image frames of our star and perform aperture photometry on each source with a radius of 15 pixels. Using AstroArt with online data, we are able to identify our target star hosting our exoplanet. The position of our target star is defined. Background data is estimated using the "Background2D" function with

a specified box size and filter size. The background data is subtracted and aperture photometry is performed using the circular aperture tool with a radius of 15 pixels. The respective aperture sums and positions are collected for each frame. A calibration function calculates and calibrates the median value of our target star's magnitude. A plot of the apparent magnitude of our target star is created with the frames on the x-axis and the normalized calibrated magnitudes on the y-axis.

Finally, numerous stars are calibrated and weighted against their median values. A variability check is completed to filter out calibrated stars that exhibit significant variability in their weighted magnitudes. A light curve of our target star and stars that passed the variability check is plotted. Another light curve of our target star is plotted with the mean calibration light curve.

4. RESULTS

4.1. *GJ-1214b*

As previously mentioned in fig. 2, our banzai images, let alone the raw images, were a major indicator of the issues that were to come when performing preliminary analysis for GJ-1214 and GJ-1214b. That is, even within our banzai images - the clean and reduced version of the raw images - were GJ-1214 and its background difficult to distinguish. Thus, when attempting to locate the number and position of stars in a single banzai images, it had printed a total of 117 stars. Had the contrast between GJ-1214 and its background been better - foreshadowing the results of WASP-14 - it would have printed a smaller list of stars - much more manageable when continuing with the next steps. Likewise, given the terrible contrast between GJ-1214 and its background this caused issues when performing aperture photometry and led to results that were not possible by any standards - and not worth mentioning in this paper in any detail. Thus, it was at this point we concluded to no longer continue forward with any sort of analysis of GJ-1214 and eventually moved onto WASP-14.

However, before continuing forth with the analysis of WASP-14, we would like to mention that GJ-1214 could have been a successful imaging target had we requested far more favorable observing parameters (e.g. longer exposure times and no filters) we may have had a successful attempt at GJ-1214. And a solution that could have, likewise, resolved the poor SNR value that was computed for GJ-1214.

4.2. *WASP-14b*

WASP14 and WASP-14b was a major success. As previously alluded to, the initial aperture photometry of a single banzai image to determine the number of stars and locate their positions led to a total of 50 stars located with WASP-14 being located at the center of the image far brighter/noticeable than its background. Likewise, proving no issue when attempting to differentiate it with its background when continuing forth with the aperture photometry for each banzai image. Thus, producing a favorable apparent magnitude plot that tracks the apparent magnitude of WASP-14 across each provided banzai image (see fig. 6).

Thereafter, we then worked on calibrating the apparent magnitude by removing any sort of variable source that far exceeded a normalized apparent magnitude value of about 1.25 since this would cause issues when attempting to calibrate the curve. Moreover, we then continue by taking the median of the remaining calibration stars in order to generate the calibration curve for the plot (see fig. 7).

It was then when we had realized that there existed outlier stars whose normalized apparent magnitudes were causing issues for further analysis. Thus, we had removed each individual star that was causing issue in order to produce favorable results. Now with the outlier stars removed, we were then able to produce the light curve and associated error bars that indicates a 0.10 dip in magnitude (see fig. 8).

4.2.1. *Error Analysis*

Systematic error: The 0.4m telescope with the sdss g filter for WASP-14 b and the 0.4m telescope with the sdss i filter for GJ-1214 b was not the best telescope. Considering that the SNR's for both planets, the issue of saturation as the LCO SNR calculator had warned was certainly a possible/present issue.

To account for the statistical error present within our WASP-14b data, error analysis is conducted on the light curves generated via python. We can find the error in our data by taking the standard deviations of our target star before transit. A static frames functions to select all images prior to transit, and the corresponding magnitudes are stored in an array. The pre-transit magnitudes are averaged, and the magnitudes are weighted differences from the mean. Statistical measurements on the magnitudes completed:

The mean is $\overline{x} = 0.9889874677498032$
The standard deviation is $\sigma = 0.016766369785125673$
The variance is $S = 0.00028111115577157507$

By removing magnitude outliers and including the standard deviation as the uncertainty for each data point, the data is plotted seen in Figure 8. We believe the statistical error to be a result of background noise,

5. DISCUSSION

Albeit the failure of GJ-1214 that was easily noted by the lack of contrast between the star and its background or the computed SNR value for the star itself, we successfully managed in producing a favorable light curve for WASP-14 that indeed compares well to current literature. Take for example fig. 9 that notes a 0.10 dip in magnitude similar to our results via their own method of transit photometry Saha (2023). Or fig. 10 that notes a 0.08 dip in magnitude Wong et al. (2015).

Further analysis of WASP-14b would possibly be to compare how well we would be able to produce known parameters of WASP-14b such as dynamical mass, eccentricity, inclination, etc. using known orbital fitting and plotting software Orvara Brandt (2023). This would first require for us to install the software from its GitHub page. Then creating a configuration file that details all the necessary stellar/planetary parameters and parameters needed for the Monte-Carlo Markov chain (mcmc) to run - the backbone of Orvara. This would in detail require for us to comb through data bases such as simbad, VizieR, and Hipparcos catalogs to name a few. The software would then be able to generate useful plots such as astrometry, orbital path, and corner plots that would be necessary to evaluate and compare our performance to existing literature containing parameters for WASP-14b.

However, as it is now, we would have certainly done a better job at our project from the start had we known what we've known now. For example, one of our many starting issues was selecting a favorable target. GJ-1214, for example, was certainly not ideal given our lack of understanding of how to properly determine the necessary filters, number of exposures, and integration time that would produce favorable images. Or, let alone select a star whose SNR would be over 700 (ideal value) and/or has a detectable magnitude - hot super Jupiters and M dwarfs (with proper filters). This was easily our main cause to our future problems aside from smaller ones such as requesting adequate time before and after transit and requesting a small window to test a target before requesting a large window.

With what we managed to achieve with a quarters-worth of independent research, we were able to use transit photometry, one of many methods to detect exoplanets, to detect the presence of WASP-14b. And with further research and analysis, this can easily be furthered by determining the parameters of the planet.

5.1. *Figures*

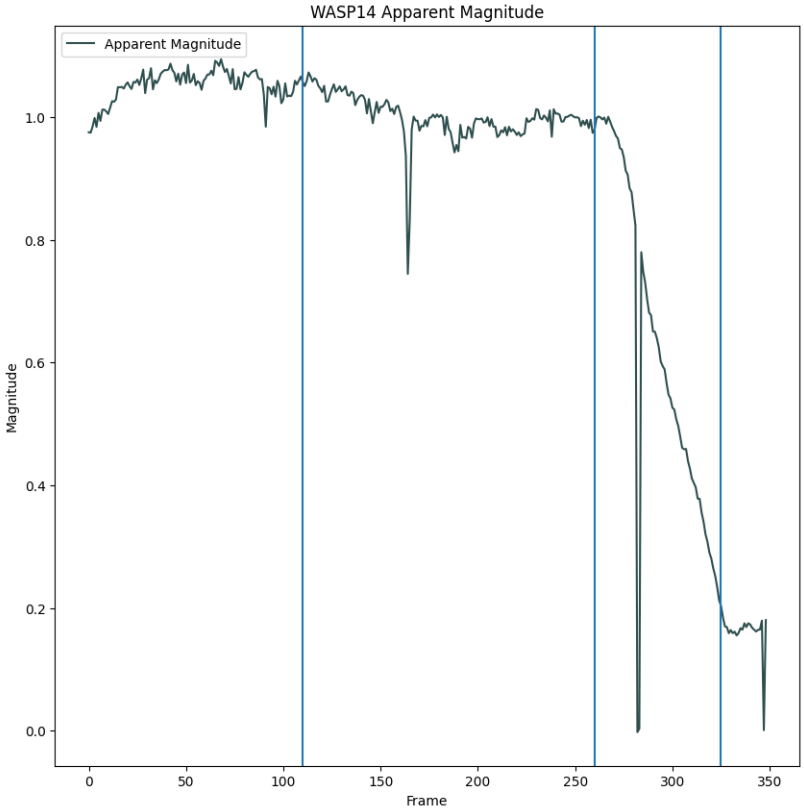

Figure 6. Plot of frames versus apparent magnitude of WASP-14 through each provided banzai image. The first vertical line is where we believe the transit begins which is a necessary parameter for the code in order to produce the following calibration curves and light curve. Likewise, the following two vertical lines are where the main transit (i.e. frames where major magnitude loss occurs) that aligns with what is present in the final light curve. (see fig. 8).

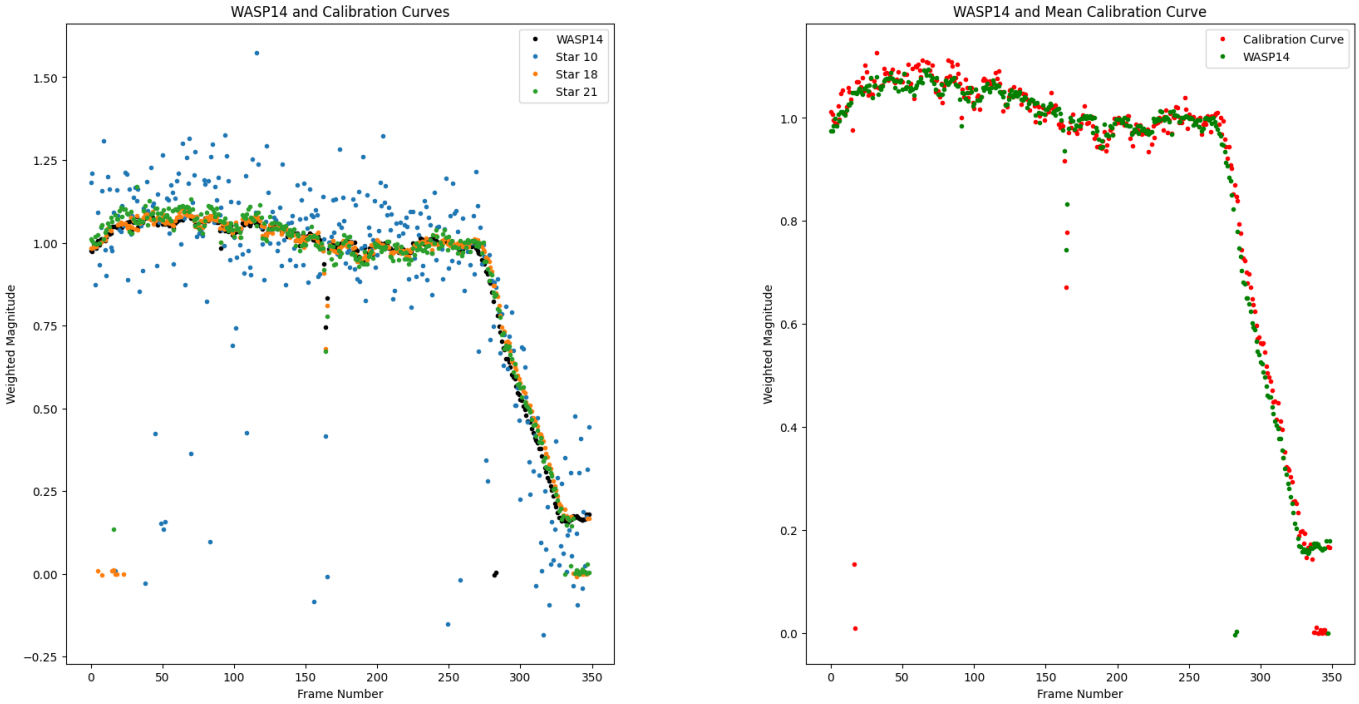

Figure 7. Plots of the calibration curve and mean calibration curve of the apparent magnitude plot (see fig. 6) of WASP-14. This was possible by removing any variable star that far exceeded a certain normalized apparent magnitude which leads to the calibration curve and by then setting calibration curve to the median of the remaining calibration stars which leads to the mean calibration curve.

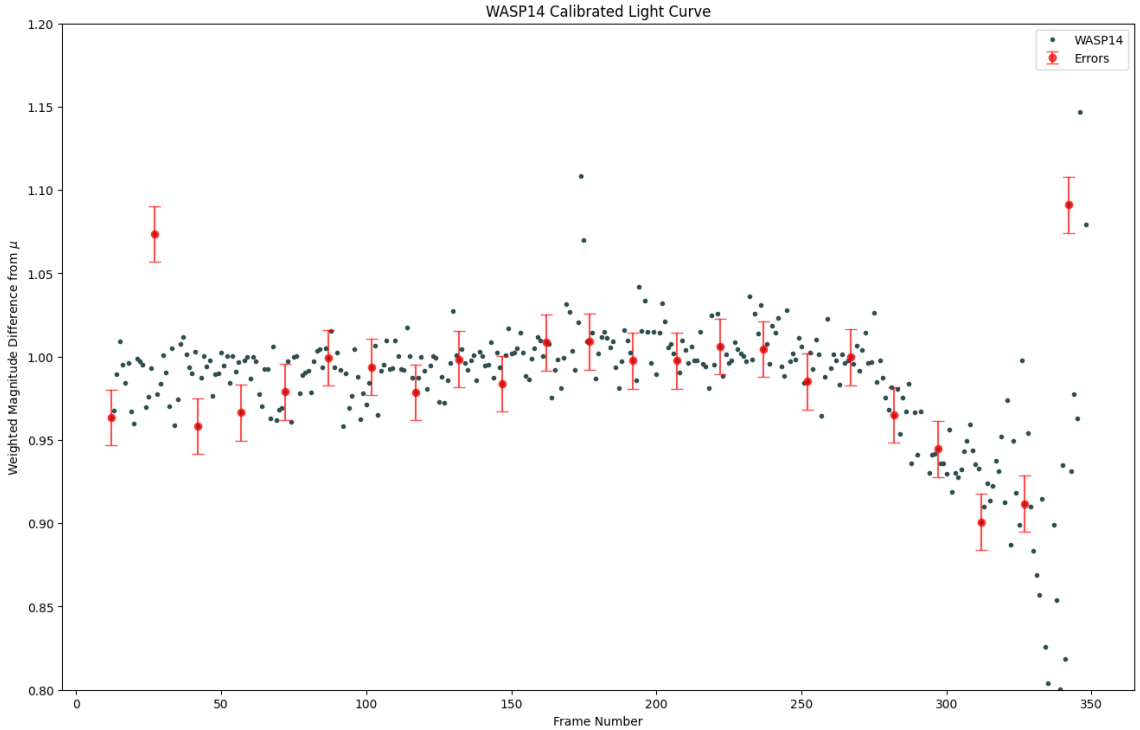

Figure 8. Final result of calibrated light curve for WASP-14 that indicates a loss of 0.10 magnitude. A sign of WASP-14b occulting the light emitted from WASP-14.

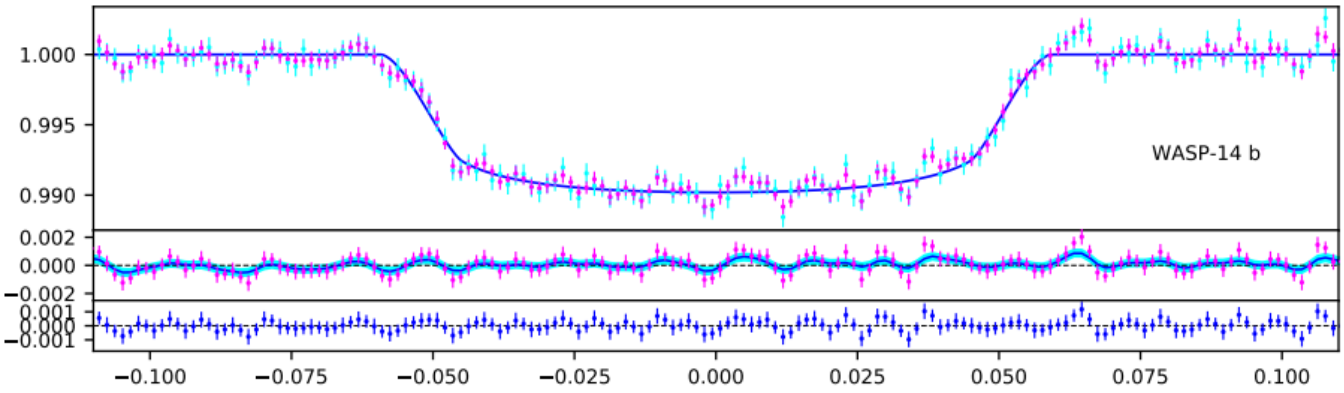

Figure 9. Best-fit light curve model that was produced by Saha (2023) indicating a 0.10 dip in magnitude.

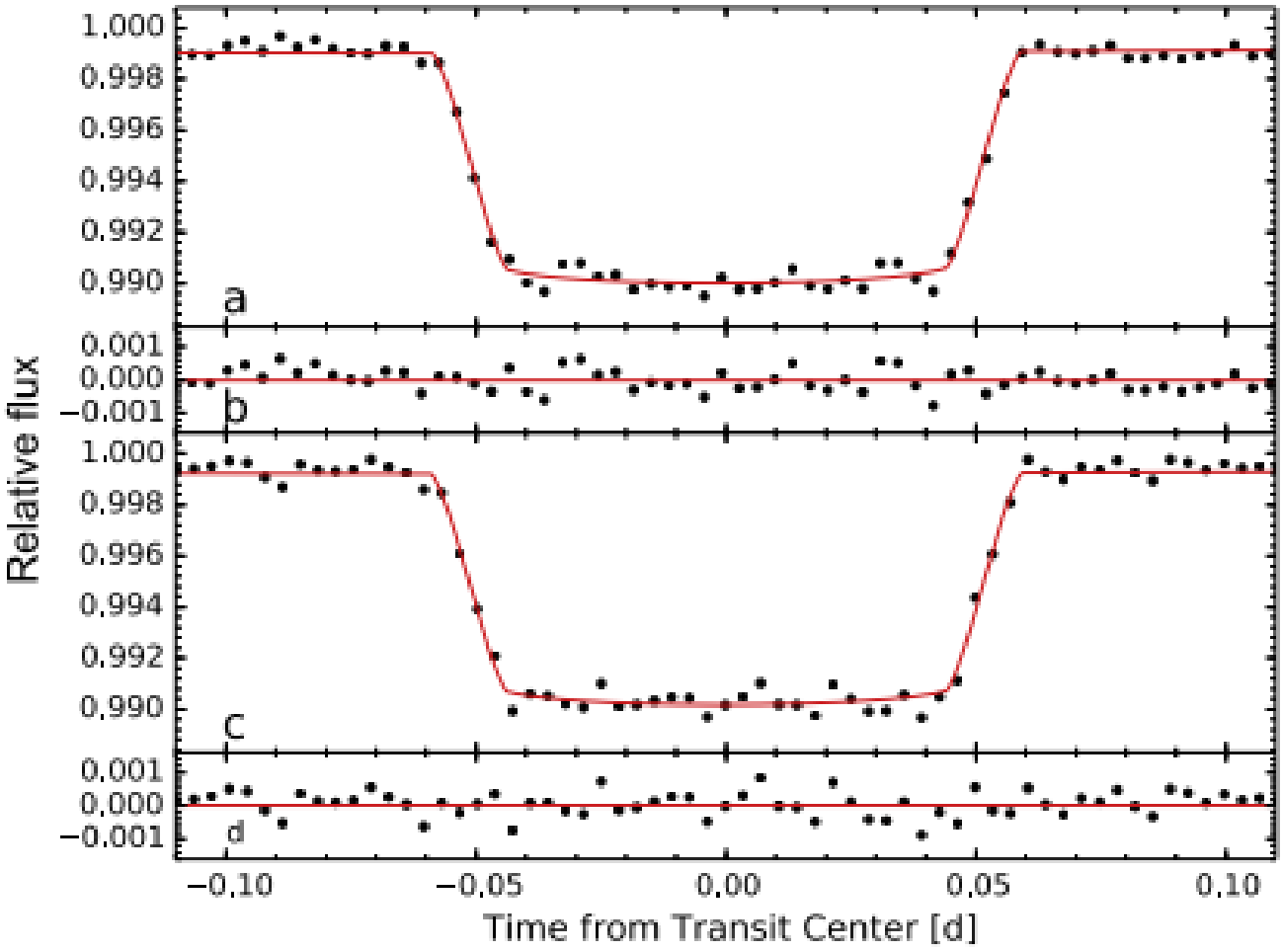

Figure 10. Best fit transit light curve produced by Wong et al. (2015) that indicates a 0.08 dip in magnitude.

REFERENCES

Afanasev, D. 2018, Detection of Exoplanets Using the Transit Method. https://arxiv.org/abs/1803.05565

Berta, Z. K., Charbonneau, D., Bean, J., et al. 2011, ApJ, 736, 12, doi: 10.1088/0004-637X/736/1/12

Brandt, T. 2023, Orvara. https://github.com/t-brandt/orvara

Charbonneau, D., Berta, Z. K., Irwin, J., et al. 2009, Nature, 462, 891, doi: 10.1038/nature08679

Exoplanet, E. 2023, Planetary Catalog. http://exoplanet.eu/

Henry, G. W., & Bean, J. L. 2023, arXiv e-prints, arXiv:2302.07874, doi: 10.48550/arXiv.2302.07874

Hood, C. E., Fortney, J. J., Line, M. R., et al. 2020, The Astronomical Journal, 160, 198, doi: 10.3847/1538-3881/abb46b

Institute, N. E. S. 2023a, NASA Exoplanet Archive. https://exoplanetarchive.ipac.caltech.edu/overview/wasp14

—. 2023b, NASA Exoplanet Archive. https://exoplanetarchive.ipac.caltech.edu/overview/gj-1214

Joshi, Y. C., Pollacco, D., Cameron, A. C., et al. 2009a, Monthly Notices of the Royal Astronomical Society, 392, 1532, doi: 10.1111/j.1365-2966.2008.14178.x

—. 2009b, Monthly Notices of the Royal Astronomical Society, 392, 1532, doi: 10.1111/j.1365-2966.2008.14178.x

(LCO), L. C. O. 2023, Visibility Tool. https://lco.global/observatory/tools/visibility/

Lubin, P. 2022, Notes for PHYS 134: Observational Astrophysics. https://www.deepspace.ucsb.edu/wp-content/uploads/2022/09/134-Notes-10-22-1.pdf

Narita, N., Nagayama, T., Suenaga, T., et al. 2013, Publications of the Astronomical Society of Japan, 65, 27, doi: 10.1093/pasj/65.2.27

NASA. 2017, Light Curves and What They Tell Us. https://avanderburg.github.io/tutorial/tutorial.html

—. 2023, Exoplanet Watch. https://exoplanets.nasa.gov/exoplanet-watch/latest-targets/

Raetz, S., Maciejewski, G., Seeliger, M., et al. 2015, MNRAS, 451, 4139, doi: 10.1093/mnras/stv1219

Saha, S. 2023, Precise Transit Photometry Using TESS: Updated Physical Properties for 28 Exoplanets Around Bright Stars. https://arxiv.org/abs/2306.02951

Society, T. P. 2023, Down in Front!: The Transit Photometry Method. https://www.planetary.org/articles/down-in-front-the-transit-photometry-method

Vanderburg, A. 2020, Transit Light Curve Tutorial. https://imagine.gsfc.nasa.gov/features/yba/M31_velocity/lightcurve/lightcurve_more.html

Wong, I., Knutson, H. A., Lewis, N. K., et al. 2015, The Astrophysical Journal, 811, 122, doi: 10.1088/0004-637X/811/2/122